

Experimental confirmation of Aharonov-Bohm effect using a toroidal magnetic field confined by a superconductor

Nobuyuki Osakabe, Tsuyoshi Matsuda, Takeshi Kawasaki, Junji Endo, and Akira Tonomura
Advanced Research Laboratory, Hitachi Ltd., Kokubunji, Tokyo 185, Japan

Shinichiro Yano and Hiroji Yamada
Central Research Laboratory, Hitachi Ltd., Kokubunji, Tokyo 185, Japan
(Received 21 January 1986)

The electron holography technique was employed to make a crucial test of the existence of the Aharonov-Bohm (AB) effect. The relative phase shift was measured between two electron waves passing through spaces inside and outside a tiny toroidal ferromagnet, covered completely with a superconductor layer and a Cu layer. Below the transition temperature the relative phase shift was measured to be 0 or π due to the magnetic-flux quantization in units of $h/2e$. The results directly demonstrated the existence of the AB effect even when the magnetic field was confined by the surrounding superconductor due to the Meissner effect and an electron beam was prevented from penetrating the magnet.

I. INTRODUCTION

The Aharonov-Bohm (AB) effect¹ has become significant as an important quantum effect.² Aharonov and Bohm predicted that an electron phase shift $\Delta\phi$ due to an electromagnetic vector potential \mathbf{A} should be observed:

$$\Delta\phi = \frac{e}{\hbar} \oint \mathbf{A} \cdot d\mathbf{s}, \quad (1.1)$$

even when the electron wave travels through a magnetic-field-free region. Since the potential \mathbf{A} is the simplest example of a gauge field, the AB effect directly shows that electromagnetism conforms to the theory of gauge fields.³⁻⁵ The AB effect has also received considerable attention from experimentalists. In the year following the prediction, the first experiment⁶ was done, followed by several other tests.⁷

Although the experimental tests supported the AB effect, the existence of the AB effect was strongly denied by Bocchieri and co-workers.⁸ They asserted that the AB effect was of purely mathematical origin. Their argument was based upon the choice of the gauge representation. A gauge transformation is generated by a scalar function f in the following manner:

$$\mathbf{A} \rightarrow \mathbf{A} + \nabla f, \quad (1.2)$$

$$\Psi \rightarrow \Psi \exp(ief/\hbar), \quad (1.3)$$

where Ψ is a wave function. They claimed that the vector potential can be eliminated, by means of a function f which generates a multivalued phase factor $\exp[(ie/\hbar)f]$, in a multiply connected field-free region. Their assertions were criticized on the basis of the single-valuedness of a wave function or on the basis of interpretation of boundary conditions in a multiply connected region.⁹

Bocchieri *et al.* also appealed to the hydrodynamical

representation of the Schrödinger equation without potentials.¹⁰ However, it was pointed out that their analysis did not represent the topological conditions. In spite of these objections the discussion of the effect continued.

They also pointed out¹¹ possible questions about the leakage of magnetic flux in previous experimental tests. Several ideas for refined experiments have been proposed. Lyuboshits *et al.*¹² suggested the use of a toroidal solenoid. Kuper¹³ proposed an experiment using a hollow superconducting torus to confine the magnetic flux. A toroidal ferromagnet was suggested by Greenberger.¹⁴

The present authors established the existence of the AB effect using a toroidal magnet without leakage flux;¹⁵ the relative phase shift observed by electron holography agreed with the theoretical estimate. However, Bocchieri *et al.*¹⁶ still argued that phase shift could be due to the Lorentz force on the portion of the electron beam passing through the magnet. In our recent experiment,¹⁷ the AB effect was confirmed using an impenetrable toroidal magnet: Au 350 nm thick was deposited on the toroid surface facing the incident electron beam. The experiment to be described here is designed to provide a crucial test of the AB effect.¹⁸ The conceptual diagram is shown in Fig. 1. An electron is strictly excluded from the magnetic field: A superconductor completely covering a toroidal magnet confines the magnetic flux by the Meissner effect. In addition, the superconductor layer and a Cu layer are thick enough to prevent electron penetration.

II. EXPERIMENTAL

A. Fabrication of toroidal magnets (Ref. 19)

A toroidal magnet covered by a superconductor is shown in Fig. 2. Three kinds of toroidal samples were fabricated for this experiment. Their sizes are listed in Table I. A small supporting branch attached to each toroid ensures thermal conductivity for cooling even

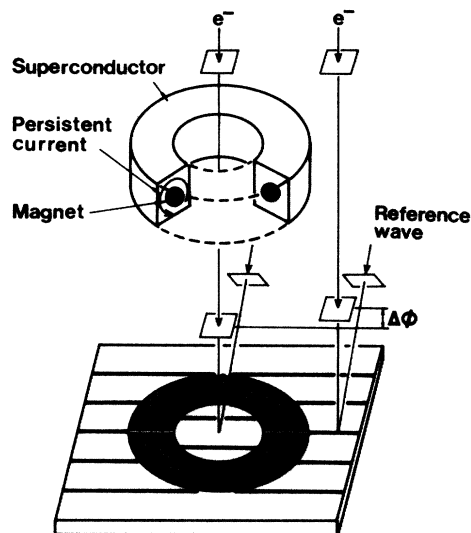


FIG. 1. Conceptual diagram of the experiment. A Cu layer for shielding from an electron wave is not shown.

under electron-beam radiation. Nb was chosen as a superconductor for the following reasons. The superconducting transition temperature is relatively high, $T_c = 9.2$ K, and the penetration depth is as small as 100 nm. Further, the processing methods for Nb have been well developed in conjunction with Josephson junction device.

The fabrication process is shown in Fig. 3. Permalloy (83 wt.% Ni–17 wt.% Fe) thin film 20 nm thick was evaporated onto a Si wafer covered with Al (300 nm thick), Nb (200 nm thick), and SiO (50 nm thick). The Al film is dissolved to peel off the completed toroid. The

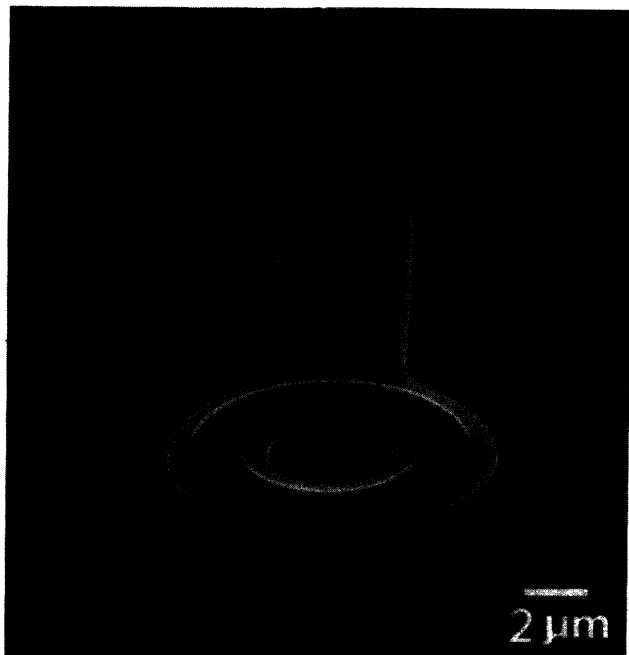


FIG. 2. Scanning electron micrograph of toroidal magnet covered by a superconductor.

TABLE I. Sizes of the toroidal magnets covered with a superconductor.

Symbol	Magnet		Superconductor	
	Inner diam (μm)	Outer diam (μm)	Inner diam (μm)	Outer diam (μm)
R1	3.0	5.0	1.5	6.5
R2	3.0	5.0	2.0	6.0
R3	3.5	5.5	2.0	7.0

SiO film reduces the coercive force of Permalloy to as low as 10 Oe, which is favorable for making a closed magnetic circuit. After deposition of the SiO layer (200 nm thick), a toroidal shape of the Permalloy sandwiched between the SiO layers was cut by ion etching. The Nb surface was cleaned by Ar^+ sputtering in order to remove a possible oxide layer [Fig. 3(a)]. The upper SiO layer protects the Permalloy toroid from Ar^+ sputtering. The film was, therefore, thinned to 50 nm in the cleaning process. After deposition of the 300-nm-thick Nb layer [Fig. 3(b)], an outer toroidal shape with a small supporting branch was cut by plasma etching [Fig. 3(c)].

Superconducting contact between the two Nb layers was checked as follows. A test device was prepared, having a contact fabricated under the same conditions as that

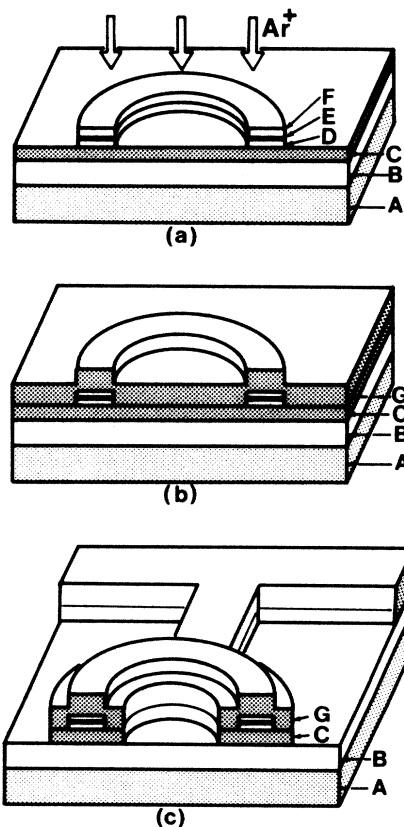


FIG. 3. Fabrication process of toroidal magnet. (a) Ar^+ sputtering for surface cleaning. (b) Sputter deposition of upper Nb layer. (c) Completed toroidal magnet. A, Si wafer; B, Al (300 nm); C, Nb (200 nm); D, SiO (50 nm); E, Permalloy (20 nm); F, SiO (200 nm); G, Nb (300 nm).

in which the toroidal sample was made. The measured critical current density through the contact at 4.2 K was $40 \text{ mA}/\mu\text{m}^2$. On the other hand, the persistent current density to quantize the magnetic flux was numerically calculated to be less than $10 \text{ mA}/\mu\text{m}^2$. The completed toroid was peeled off from the Si wafer by dissolving the Al layer in NaOH solution and was placed on a Cu mesh.

Finally, Cu was evaporated onto all the surfaces to avoid both charging-up and contact-potential effects: (a) An oxide layer of the Nb surface formed in the air would destroy a charge balance under electron beam radiation possibly because of the charge storage due to its low conductivity or overemission of secondary electrons. It produces electric fields around the toroidal sample. (b) The potential difference appears when the two different metals, Nb of the toroid and Cu of the mesh, are connected. The value is equal to the difference between the two work functions. The potential difference of 1 V between the toroid and the mesh produces the phase shift of π between two electron beams, one near the edge of the toroid and the other $3 \mu\text{m}$ apart from it.

B. Cooling apparatus

A cross-sectional diagram of an electron microscope with cooling apparatus is shown in Fig. 4. A liquid-He reservoir *B* is attached to the column. The toroidal sample is placed at the cooling stage *C* in the column, which is shown in Fig. 5. The stage consists of three cooling parts for both radiation and condensation protection. Part *A* is cooled by liquid N_2 and the two inner parts, *B* and *C*, are cooled by liquid He. Each part is connected to a conduction rod *D* from the reservoir through a cylindrical Ag foil with many slits for flexibility *E*. A specimen

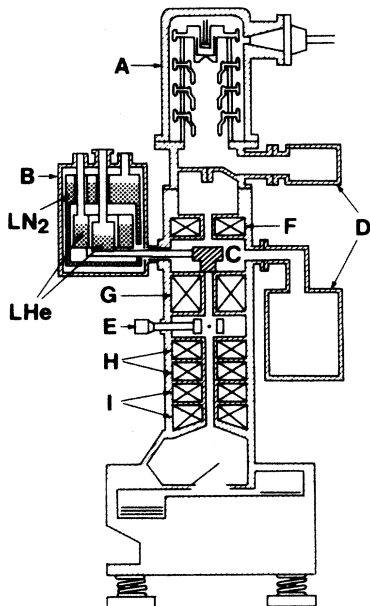


FIG. 4. Cross section of electron microscope with cooling apparatus. *A*, field emission gun; *B*, liquid-He reservoir; *C*, cooling stage; *D*, ion pumps; *E*, biprism; *F*, condenser lens; *G*, objective lens; *H*, intermediate lenses; *I*, projector lenses.

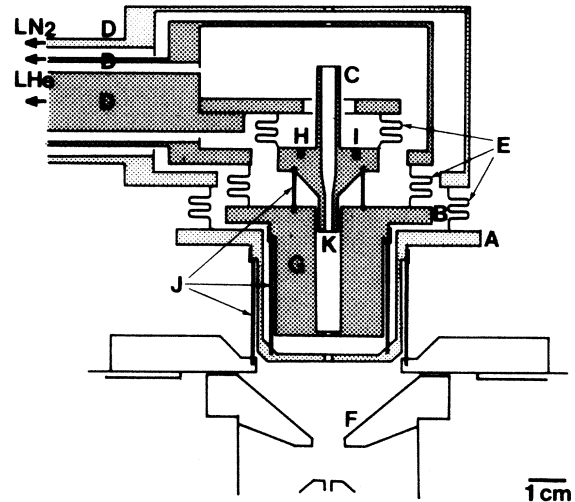


FIG. 5. Cross section of cooling stage. *A*, second shield; *B*, first shield; *C*, specimen holder; *D*, conducting rods; *E*, heater; *F*, objective pole-piece; *G*, superconducting coil; *H*, heater; *I*, Ge resistor; *J*, insulating supports; *K*, specimen.

is placed in part *C* (specimen holder). Thermal contact is given careful attention. A tiny In ring is inserted between the specimen and the holder. They are clamped by a screw cap. The temperature is controlled by a heater *H*, and measured by a calibrated Ge resistor *I* (Scientific Instruments, Inc.). The temperature can be controlled with the precision $\Delta T/T < 10^{-3}$ in the temperature range below 50 K. However, the apparatus is incapable of keeping a specimen at a constant temperature higher than 50 K because of rapid evaporation of liquid He. A magnetic field can be applied using a superconducting coil *G*.

The temperature difference between the toroid and the holder is estimated to be less than 0.1 K under the following assumptions: The current density of a 150-kV electron beam is $1 \times 10^{-5} \text{ A}/\text{cm}^2$, the energy of all the electrons hit the toroid changes into the thermal energy, and the thermal conductivity of Nb is $0.2 \text{ W}/\text{cm K}$. It was also confirmed experimentally that the difference was less than 0.5 K. The superconducting transition temperature $T_c = 9.2 \text{ K}$ of Nb was compared to that of a holder when a trapped magnetic flux in a hole of Nb film leaked.

Careful attention was paid to the cooling procedure to prevent gas condensation onto the sample, which would create potential differences through charging up. The specimen holder was kept at room temperature until part *B* cooled to 20 K, where all the residual gases except Ne, H, and He were condensed onto part *B*. Further, part *B* was cooled to 5 K while the specimen holder was kept at 20 K for Ne condensation. Finally the specimen was cooled to liquid-He temperature. The gas from an electron beam line was reduced by inserting two apertures cooled by liquid N_2 into objective and projector lenses.

C. Electron holography

Relative phase-shift detection was carried out by measuring that of an optically reconstructed wave from an electron hologram. The off-axis image hologram was

formed in a Hitachi H-800 electron microscope installed with a field emission gun²⁰ (Fig. 4), which provided a coherent electron beam.

Electrons were emitted from a cold (310)-oriented tungsten tip, through the application of a 3–5-kV electric potential between the tip and the first anode. The total emission current was a few tenths of μA , while only a several nA electron beam along the optical axis was fed through apertures to form a hologram in order to eliminate electrons having trajectories distorted by the aberrations of the accelerating lenses. The electron was accelerated to 150 kV through a six-stage accelerating tube to form a collimated beam. Illuminating condition (beam divergence angle α and current density j) was controlled by a condenser lens and an aperture.

Electron optical system for the hologram formation is shown in Fig. 6. Only a half plane of a specimen position was used. The other half was used for the reference beam. The image of the specimen was formed on a photographic film with the magnification of 1000 times. A Möllenstedt-type electron biprism, located between an objective and intermediate lenses, was employed to overlap an object wave and a reference wave to form a hologram.

The beam current density and exposure time were restricted by coherence conditions of the electron beam and stability of the apparatus. The beam current density at the specimen was set to range from 1×10^{-6} to 5×10^{-6} A/cm² and the exposure time was 10–30 sec. With these parameters, the density of the electron beam is such that on the average there is only one electron in the microscope column. The specimen temperature is not influenced by the beam radiation within the beam current range as

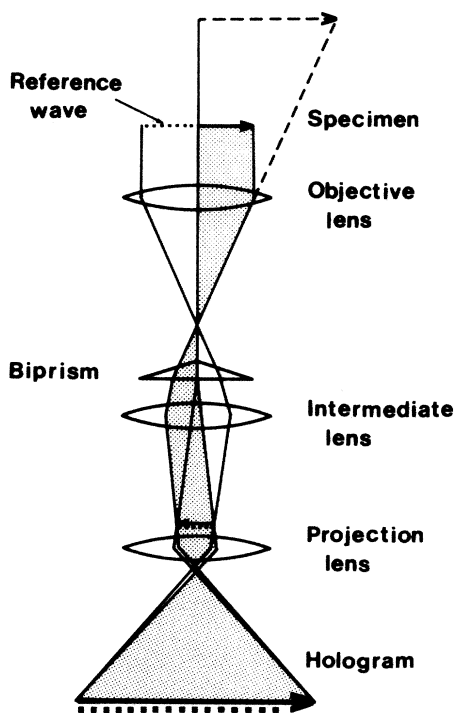


FIG. 6. Schematic diagram of hologram formation.

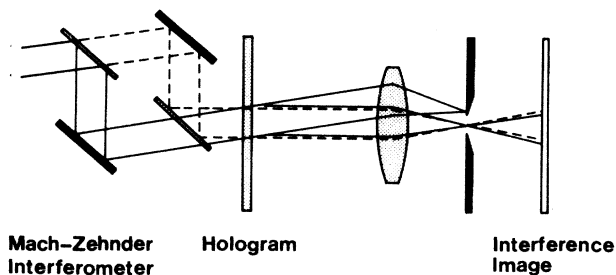


FIG. 7. Optical reconstruction system for interference microscopy.

described in Sec. II B. Actually the result was independent of the value of the current density.

Optical reconstruction and relative phase-shift measurement were carried out through use of the setup shown in Fig. 7. A pair of collimated He-Ne laser beams (wave length, 633 nm) made by Mach-Zehnder interferometer illuminated the hologram. Each beam produced the reconstructed image and its conjugate. The reconstructed image of one beam was superposed onto the transmitted wave of the other wave to produce a standard interference micrograph. The reconstructed and the conjugate images of each beam were used for a doubly phase-amplified interference micrograph.²¹

Here, two types of interference images are used: a contour map and an interferogram. The former is obtained by setting the reconstructed and the transmitted (conjugate, in case of double phase amplification) waves parallel as illustrated in Fig. 7, which represents a contour map of relative phase-shift distribution. If the object is a magnetic field, the contour lines indicate projected magnetic lines of force.²² There, constant fluxes of h/e and $h/2e$ flow between two adjacent contour lines in standard and doubly phase-amplified images, respectively. The latter, i.e., the interferogram, is obtained by tilting the two waves to each other. The interference fringe spacing depends on the angle between the beams ($\sim 10^{-3}$ rad), however it does not affect the result because the relative phase shift was measured as a relative displacement to a regular fringe spacing.

III. RESULTS

A. Studies above T_c

Fabricated toroidal magnets were examined at room temperature to select ones with closed magnetic circuits. Contour maps in Fig. 8 show examples of toroids with and without leakage magnetic flux. In Fig. 8(a) the presence of the magnetic poles are clearly seen at the upper right of the toroid and its opposite position, where the magnetic lines of force emerge. The toroidal magnet consists of two magnetic domains having opposite magnetization directions. On the other hand, no fields can be seen around the toroid 8(b), substantiating a closed magnetic circuit.

Whether a closed magnetic circuit is formed or not depends on the toroid's thickness and diameter. It was confirmed from the experiment that optimum thickness was

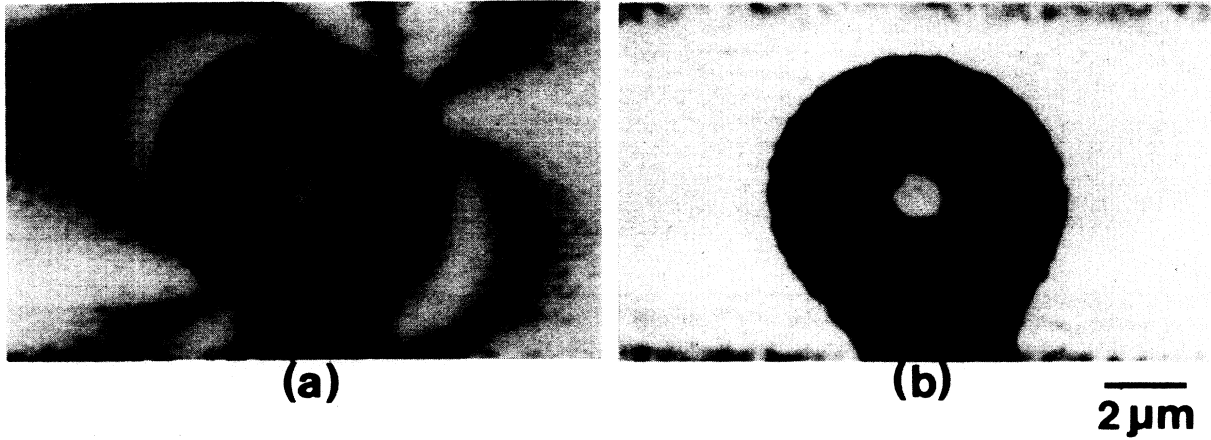


FIG. 8. Contour maps of toroidal magnets at room temperature. (a) Toroid with leakage field (phase amplification, $\times 2$). (b) Toroid without leakage field (phase amplification, $\times 2$).

20 nm, and smaller diameter was favorable for producing a closed circuit. Approximately 60% of all the toroids fabricated formed closed circuit for the dimension employed in this experiment.

When the toroid was cooled from room temperature, the phase-shift value was detected to change. This is explained using the Weiss theory of ferromagnetism, predicting that spin orientation in the Permalloy is aligned due to the reduction of thermal vibration. Therefore, spontaneous magnetization increases to change the phase-shift value. The change of measured phase shift for 20 toroidal magnets is shown in Fig. 9. The cross sections of the toroids were so designed as to have the same dimensions, $1 \mu\text{m}$ wide and 20 nm thick. The width fluctuates $\pm 0.1 \mu\text{m}$ due to the precision of a photo mask. This is the reason why phase shift varies from sample to sample. The measured difference between the phase shift at 15 K, $\Delta\phi_{15 \text{ K}}$, and the phase shift at 300 K, $\Delta\phi_{300 \text{ K}}$, is given by the following equation:

$$\Delta\phi_{15 \text{ K}} - \Delta\phi_{300 \text{ K}} = \pm 0.45\pi + 2n\pi,$$

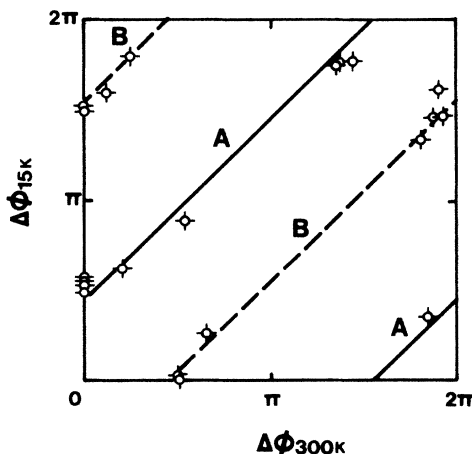


FIG. 9. Relation between relative phase shift at 300 K ($\Delta\phi_{300 \text{ K}}$) and at 15 K ($\Delta\phi_{15 \text{ K}}$).

where the term $2n\pi$ is trivial, and can be eliminated by gauge transformation. The positive and negative signs in the first term of the right side corresponding to the lines *A* and *B* in Fig. 9 are due to the different directions of the rotation of the magnetization. The value $0.45\pi \pm 0.05\pi$ can be well explained as follows: According to the experimental data by Crangle and Hallam,²³ the magnetization of the Permalloy of the composition employed here increases by 5% when cooled from 300 to 15 K. The amount of the total flux confined in a toroid at 300 K is approximately $5(h/e)$ ($M_s = 0.95 \text{ T}$; cross section is $1 \mu\text{m} \times 20 \text{ nm}$.) Then the relative phase-shift change is 0.5π . Thus it is clearly demonstrated that the relative phase shift is controlled by the magnetic flux confined in the toroid.

B. Studies below T_c

The toroids were further cooled below T_c for magnetic shielding by the Meissner effect. The superconducting state of Nb was confirmed through observation of the flux quantization.²⁴

Figures 10(b) and 10(e) are doubly phase-amplified interferograms of two toroids cooled at 5 K. There is no relative displacement between the fringes inside and outside the rings, i.e., the images of the toroids, while displacements are seen in the interferograms of the toroids cooled at 15 K [Figs. 10(a) and 10(d)]. Therefore, the phase shifts at 5 K are integral multiples of π , consistent with the quantization of the confined flux in units of $h/2e$.²⁵ The transition was observed to take place reversibly at $9 \text{ K} \pm 1 \text{ K}$, which is good agreement with the superconducting transition of Nb ($T_c = 9.2 \text{ K}$).

In standard interferograms, i.e., interferograms without phase amplification, it can be counted whether the n , the multiplication number of the unit flux $h/2e$, is even or odd. In case of odd n , the relative phase shift is π , and the shift is 0 for even n . Thus, they are distinguished as just half-spacing displacement [Fig. 10(f)] and no displacement [Fig. 10(c)]. Further evidence for the supercon-

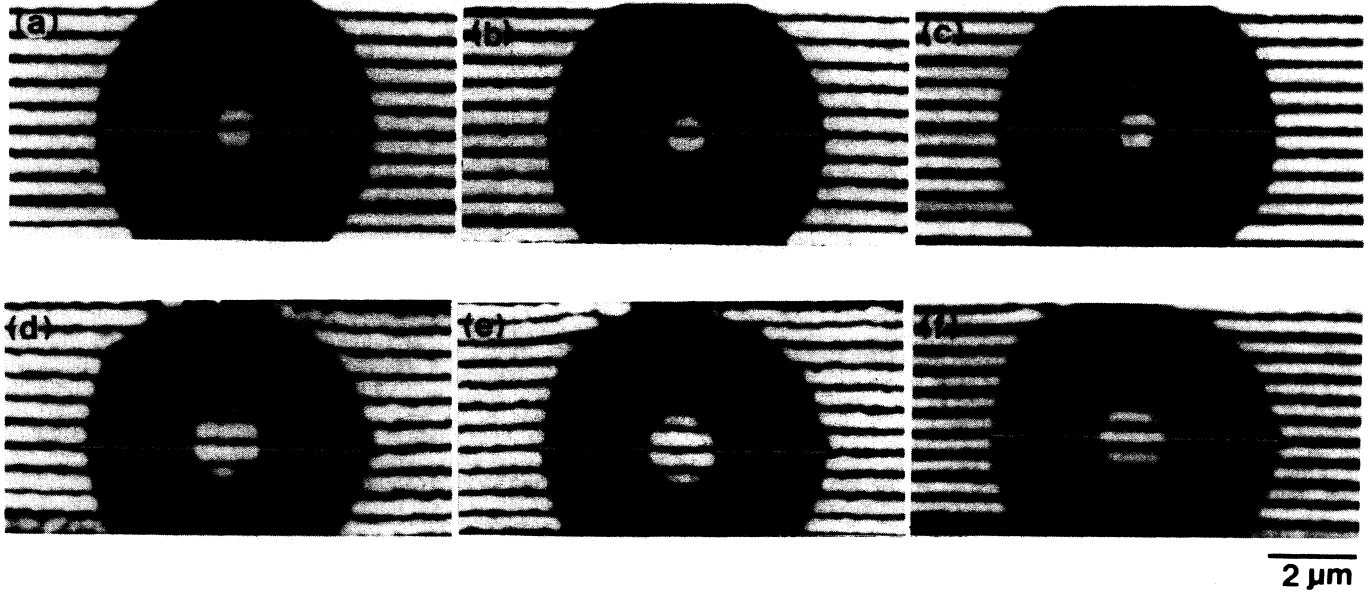


FIG. 10. Interferograms of toroids at 15 and 5 K. (a), (b), and (c): magnetic flux is quantized in $n(h/2e)$ (n is even) below T_c . The toroid is R1 (see Table I); (d), (e), and (f): magnetic flux is quantized in $n(h/2e)$ (n is odd) below T_c . The toroid is R2. (a) and (d), $T=15$ K (phase amplification, $\times 2$). (b) and (e), $T=5$ K (phase amplification, $\times 2$). (c) and (f), $T=5$ K (phase amplification, $\times 1$).

ducting transition are given by comparing the phase shift below T_c (0 or π) and above T_c ($0-2\pi$). In Fig. 11, the phase-shift change is consistent with the theoretically predicted relationship shown by the dotted line. The flux quantization occurs so as to minimize the Gibbs free energy. Energy of the magnetic field to add for quantizing the flux is minimized.

The observations described above substantiate the superconducting state of the surrounding Nb layer, which confines the magnetic flux. Then the observed relative phase shift π in the case of odd n clearly demonstrates the existence of the AB effect.

IV. DISCUSSION AND CONCLUSION

A magnetic field produced by the objective pole piece would be the primary magnetic source except the toroidal

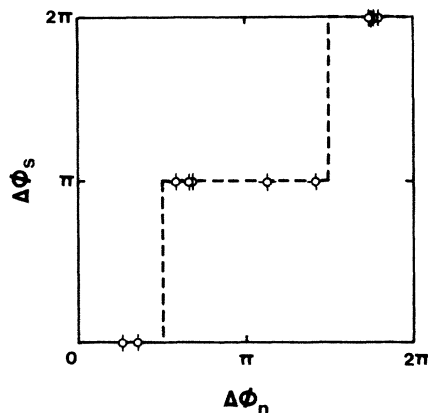


FIG. 11. Relation between relative phase shift below T_c ($\Delta\phi_s$) and above T_c ($\Delta\phi_n$).

magnet. To reduce the field, the specimen was separated from the gap center of the pole piece by 6 cm, and the objective lens was used at weak excitation as small as 1000 ampere turn. Estimated magnetic flux flowing through the toroidal hole is less than $h/100e$. The magnetic field originated outside the microscope was shielded by a 5-cm-thick μ -metal column, and only a field of an order of μ G remained.

Further, we confirmed experimentally that interference fringes were not shifted in our setting if nonmagnetic specimen were introduced at 5 K and at room temperature. A test specimen was fabricated, which was identical to the specimen except that it had no Permalloy toroidal magnet. It was prepared in the same way as the specimen for holographic measurement. Resultant interferograms of both double and standard phase amplifications are shown in Fig. 12. No relative phase shift was detected between inside and outside the toroid in the measurement precision of $h/50e$.

Electron beam touching the magnetic field was noted¹⁶ as possible cause of the fringe shift in our previous experiment.¹⁵ The portion of electrons penetrating through the Cu and Nb layers is estimated. Only coherently transmitting electrons are evaluated here, as possible contributors to the formation of the interference fringes. Further, both plasmon and core-electron excitations are considered to be incoherent scattering. Under these assumptions, the optical potential method²⁶ is employed with the potential value numerically calculated by Radi.²⁷ The relative intensity of electrons penetrating to meet the magnetic flux is thus estimated to be 5×10^{-6} from thicknesses 300 and 100 nm of Nb and Cu layers and from the penetration depth 100 nm of the magnetic flux into Nb; the shielding by the Nb and Cu layers is considered to be satisfactory.

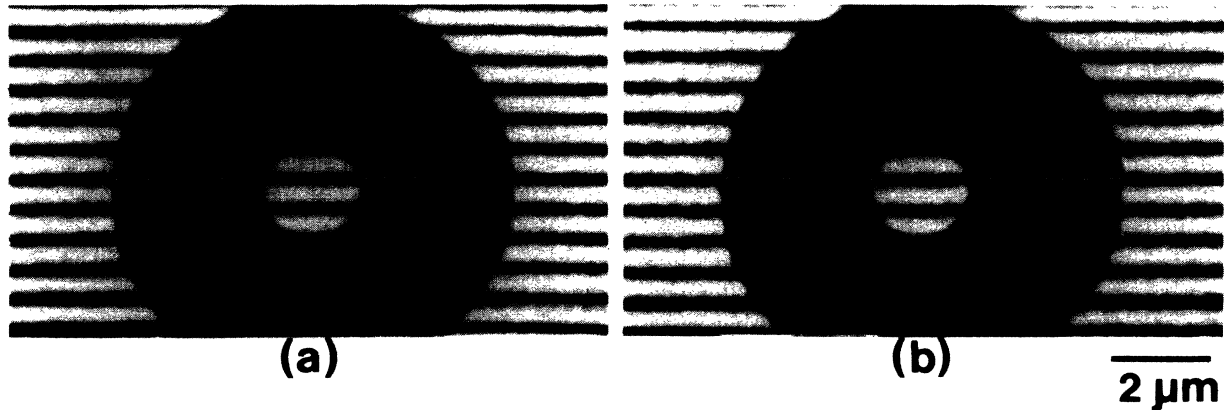


FIG. 12. Interferograms of toroid without magnet. (a) Phase amplification, $\times 1$. (b) Phase amplification, $\times 2$.

Sufficient shielding from electron penetration was also supported by the experimental results in which the change in Cu layer thickness from 50 to 200 nm had no effect in interference fringes around the quantized magnetic flux.

The leakage flux from the magnet, if any, would cause interaction between electron waves and the magnetic field. However, it could be shielded by a superconducting Nb layer by the Meissner effect. It is estimated that the leakage flux is far less than $h/200e$, since the leakage flux just above the transition temperature is less than $h/20e$ and the minimum thickness and London penetration depth of Nb are 250 and 100 nm, respectively.

In conclusion, the existence of the AB effect was confirmed under the conditions of no leakage field and of no electron penetration. It was also supported by observation of the expected dependence of the relative phase shift to the magnetic flux confirmed through temperature dependence of spontaneous magnetization.

ACKNOWLEDGMENTS

The authors are grateful to Professor Chen Ning Yang of the State University of New York for giving them the idea for this experiment, which was proposed at the International Symposium on Foundations on Quantum Mechanics, 1983. They wish to acknowledge Professor Tatsuo Arie of The National Institute for Physiological Sciences for his cooperation and advice on the magnetism of Permalloy ring. They are indebted to Dr. Ushio Kawabe of Hitachi, Ltd. for his valuable discussion on experiment design and results. They also wish to acknowledge Mr. Mikio Hirano of Hitachi, Ltd. for his valuable advice on the toroid fabrication and preparation of electron holography measurements. They gratefully acknowledge the valuable discussions and advice in preparing this manuscript given by Dr. Akira Fukuhara of Hitachi, Ltd. and Professor Hiroshi Ezawa of Gakushuin University.

¹Y. Aharonov and D. Bohm, *Phys. Rev.* **115**, 485 (1959).

²S. Olariu and I. I. Popescu, *Rev. Mod. Phys.* **57**, 339 (1985).

This paper reviewed the recent discussions on the AB effect.

³T. T. Wu and C. N. Yang, *Phys. Rev. D* **12**, 3845 (1975).

⁴J. Anandan, *Proceedings of the Conference on Differential Geometric Method in Theoretical Physics, Trieste, 1981* (World Scientific, Singapore, 1983).

⁵M. Peshkin, I. Talmi, and L. J. Tassie, *Ann. Phys.* **16**, 426 (1960).

⁶R. G. Chambers, *Phys. Rev. Lett.* **5**, 3 (1960).

⁷H. A. Fowler, L. Marton, J. A. Simpson, and J. A. Suddeth, *J. Appl. Phys.* **32**, 1153 (1961); H. Boersch, H. Hamisch, K. Grohmann, and D. Wohlleben, *Z. Phys.* **165**, 79 (1961); G. Möllenstedt and W. Bayh, *Phys. Bl.* **18**, 299 (1962).

⁸P. Bocchieri and A. Loinger, *Nuovo Cimento* **47A**, 475 (1978); P. Bocchieri, A. Loinger, and G. Siragusa, *ibid.* **56A**, 55 (1980).

⁹U. Klein, *Lett. Nuovo Cimento* **25**, 33 (1979); D. Bohm and B. J. Hiley, *Nuovo Cimento* **52A**, 295 (1979); D. M. Greenberger, *Phys. Rev. D* **23**, 1460 (1981).

¹⁰F. Strocchi and A. S. Wightman, *J. Math. Phys.* **15**, 2189 (1974).

¹¹S. M. Roy, *Phys. Rev. Lett.* **44**, 111 (1980).

¹²V. H. Lyuboshits and Y. A. A. Smorodinskii, *Zh. Eksp. Teor. Fiz.* **75**, 40 (1978) [*Sov. Phys.—JETP* **48**, 19 (1978)].

¹³C. G. Kuper, *Phys. Lett.* **79A**, 413 (1980).

¹⁴D. M. Greenberger, *Phys. Rev. D* **23**, 1460 (1981).

¹⁵A. Tonomura, T. Matsuda, R. Suzuki, A. Fukuhara, N. Osakabe, H. Umezaki, J. Endo, K. Shinagawa, Y. Sugita, and H. Fujiwara, *Phys. Rev. Lett.* **48**, 1143 (1982).

¹⁶P. Bocchieri, A. Loinger, and G. Siragusa, *Lett. Nuovo Cimento* **35**, 370 (1982).

¹⁷A. Tonomura, H. Umezaki, T. Matsuda, N. Osakabe, J. Endo, and Y. Sugita, *Proceedings of the International Symposium on Foundations on Quantum Mechanics, Tokyo, 1983* (Physical Society of Japan, Tokyo, 1984), p. 20. Mollenstedt *et al.* tested the AB effect using a solenoid in a glass tube: G. Möllenstedt, H. Schmid, and H. Lichte, *Proceedings of the International Congress on Electron Microscopy, Hamburg, 1982* (Deutsche Gesellschaft für Elektronen mikroskopie eV., Frankfurt, 1982), Vol. 1, p. 733.

¹⁸A. Tonomura, N. Osakabe, T. Matsuda, T. Kawasaki, J. Endo, S. Yano, and H. Yamada, *Phys. Rev. Lett.* **56**, 792 (1986).

- ¹⁹The detailed description of the toroid will be submitted by S. Yano *et al.* (unpublished).
- ²⁰A. Tonomura, T. Matsuda, J. Endo, H. Todokoro, and T. Komoda, *J. Electron Microsc.* **28**, 1 (1979).
- ²¹J. Endo, T. Matsuda, and A. Tonomura, *Jpn. J. Appl. Phys.* **18**, 2291 (1979).
- ²²A. Tonomura, T. Matsuda, H. Tanabe, N. Osakabe, J. Endo, A. Fukuhara, K. Shinagawa, and H. Fujiwara, *Phys. Rev. B* **25**, 6799 (1982); T. Matsuda, A. Tonomura, R. Suzuki, J. Endo, N. Osakabe, H. Umezaki, H. Tanabe, Y. Sugita, and H. Fujiwara, *J. Appl. Phys.* **53**, 5444 (1982); N. Osakabe, K. Yoshida, Y. Horiuchi, T. Matsuda, H. Tanabe, T. Okuwaki, J. Endo, H. Fujiwara, and A. Tonomura, *Appl. Phys. Lett.* **42**, 746 (1983).
- ²³J. Crangle and G. C. Hallam, *Proc. R. Soc. London* **272**, 119 (1963).
- ²⁴The quantization of the trapped flux in a hollow superconducting cylinder was detected by electron interferometry: B. Lischke, *Phys. Rev. Lett.* **22**, 1366 (1969); H. Boersch and B. Lischke, *Z. Phys.* **237**, 449 (1970); B. Lischke, *ibid.* **237**, 469 (1970); **239**, 360 (1970); H. Wahl, *Optik (Stuttgart)* **30**, 508; H. Wahl, *ibid.* **30**, 577 (1970).
- ²⁵The Nb layer was confirmed from the numerical calculation to be thick enough that the fluxoid quantization results in the flux quantization.
- ²⁶H. Yoshioka, *J. Phys. Soc. Jpn.* **12**, 618 (1957).
- ²⁷G. Radi, *Acta Crystallogr. A* **26**, 41 (1970).

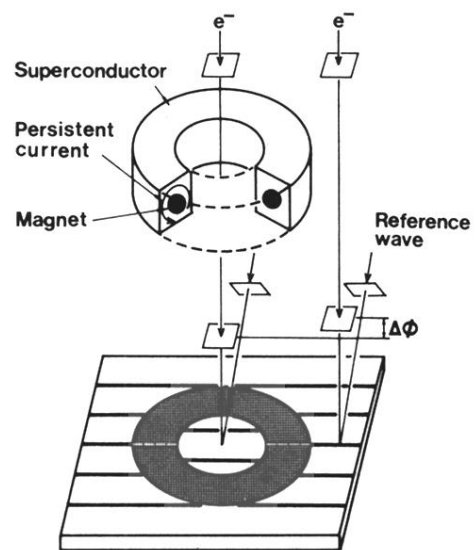


FIG. 1. Conceptual diagram of the experiment. A Cu layer for shielding from an electron wave is not shown.

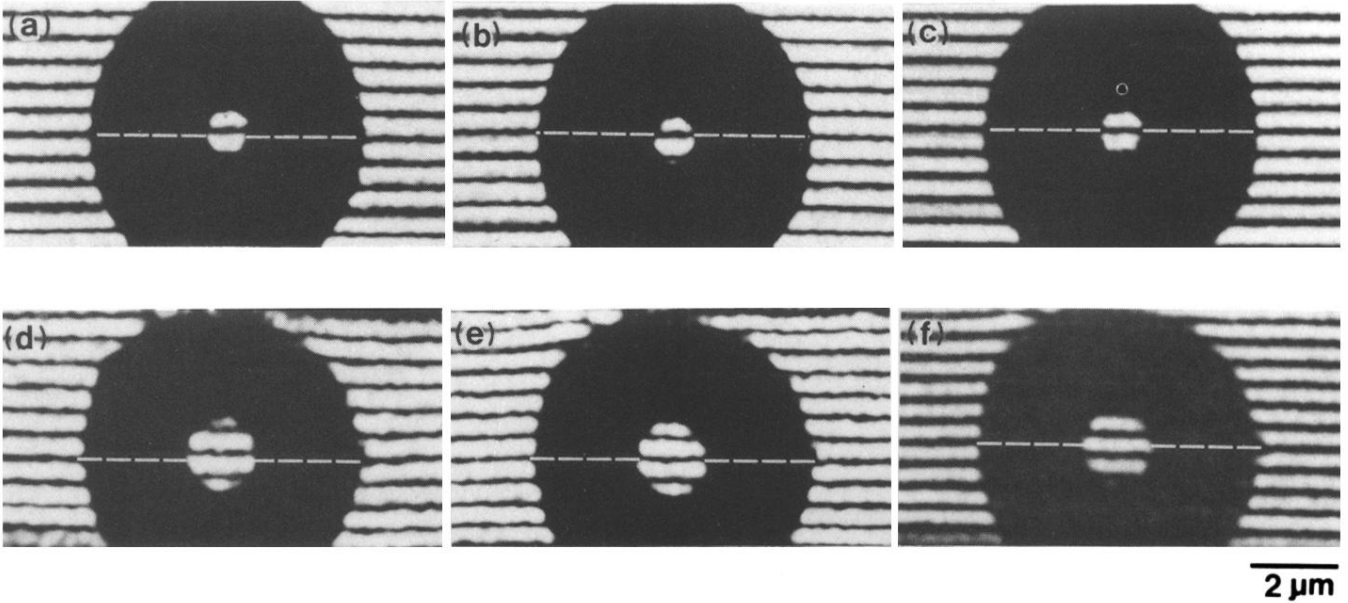


FIG. 10. Interferograms of toroids at 15 and 5 K. (a), (b), and (c): magnetic flux is quantized in $n(h/2e)$ (n is even) below T_c . The toroid is *R1* (see Table I); (d), (e), and (f): magnetic flux is quantized in $n(h/2e)$ (n is odd) below T_c . The toroid is *R2*. (a) and (d), $T=15$ K (phase amplification, $\times 2$). (b) and (e), $T=5$ K (phase amplification, $\times 2$). (c) and (f), $T=5$ K (phase amplification, $\times 1$).

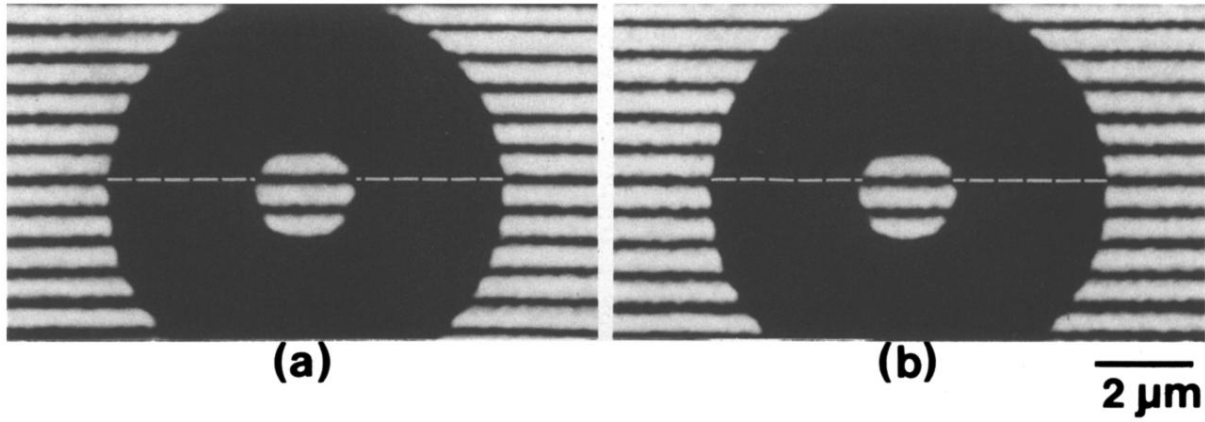


FIG. 12. Interferograms of toroid without magnet. (a) Phase amplification, $\times 1$. (b) Phase amplification, $\times 2$.

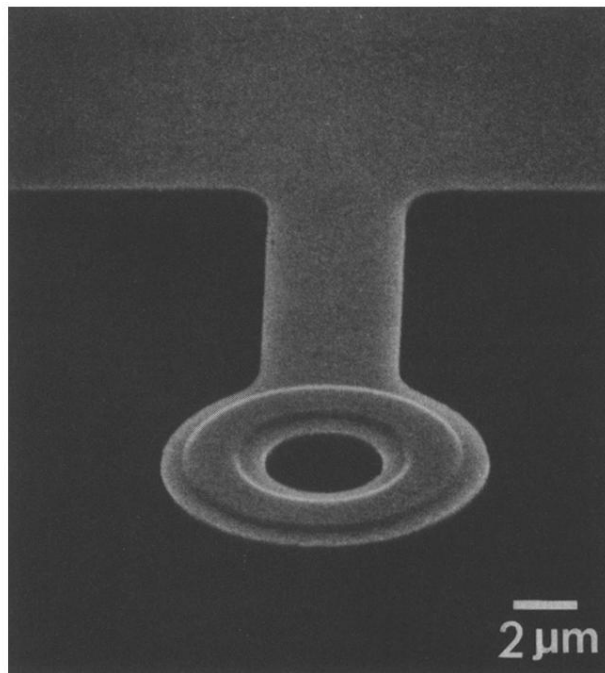


FIG. 2. Scanning electron micrograph of toroidal magnet covered by a superconductor.

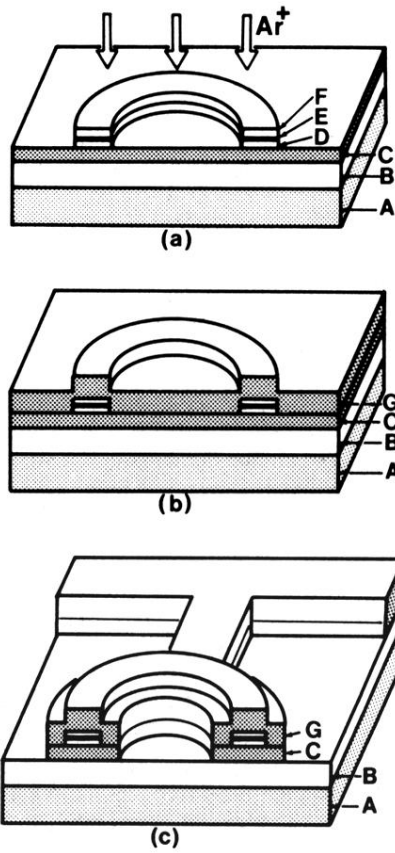


FIG. 3. Fabrication process of toroidal magnet. (a) Ar^+ sputtering for surface cleaning. (b) Sputter deposition of upper Nb layer. (c) Completed toroidal magnet. *A*, Si wafer; *B*, Al (300 nm); *C*, Nb (200 nm); *D*, SiO (50 nm); *E*, Permalloy (20 nm); *F*, SiO (200 nm); *G*, Nb (300 nm).

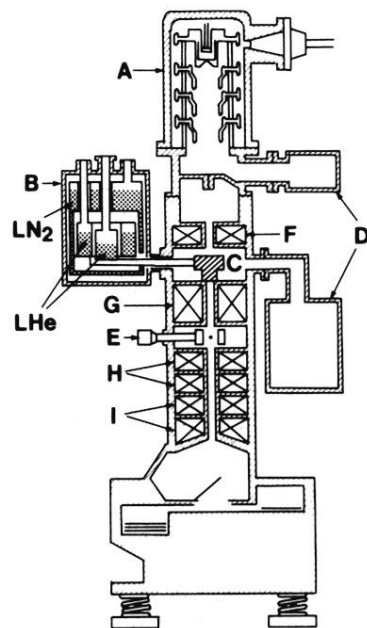


FIG. 4. Cross section of electron microscope with cooling apparatus. *A*, field emission gun; *B*, liquid-He reservoir; *C*, cooling stage; *D*, ion pumps; *E*, biprism; *F*, condenser lens; *G*, objective lens; *H*, intermediate lenses; *I*, projector lenses.

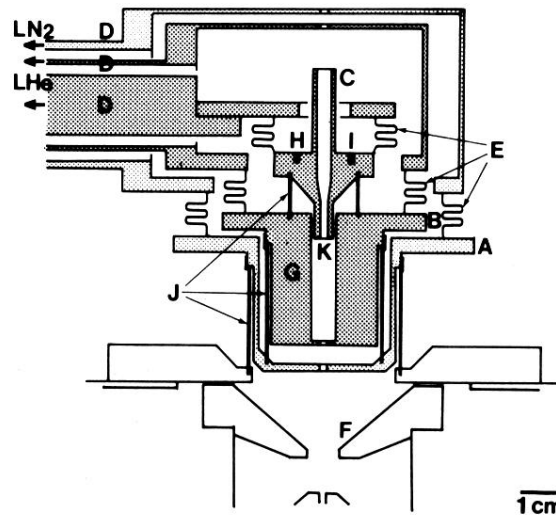


FIG. 5. Cross section of cooling stage. *A*, second shield; *B*, first shield; *C*, specimen holder; *D*, conducting rods; *E*, heater; *F*, objective pole-piece; *G*, superconducting coil; *H*, heater; *I*, Ge resistor; *J*, insulating supports; *K*, specimen.

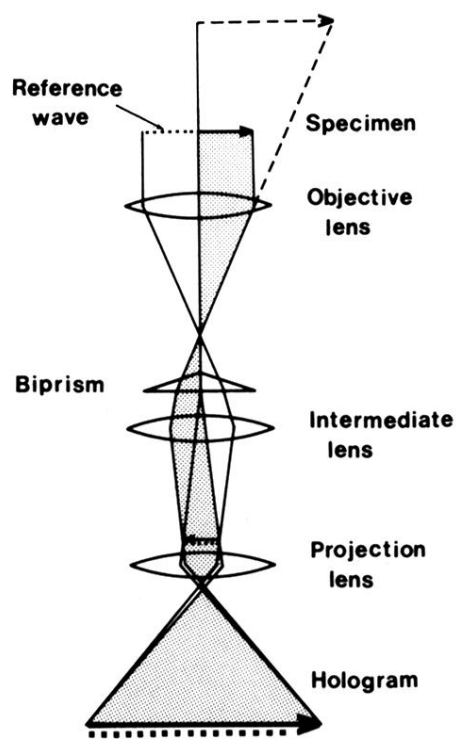
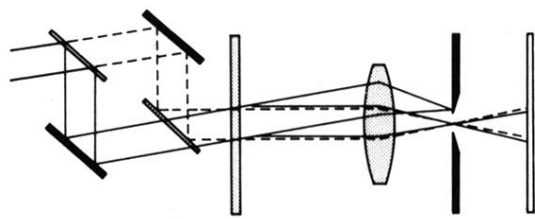


FIG. 6. Schematic diagram of hologram formation.



Mach-Zehnder Interferometer **Hologram** **Interference Image**

FIG. 7. Optical reconstruction system for interference microscopy.

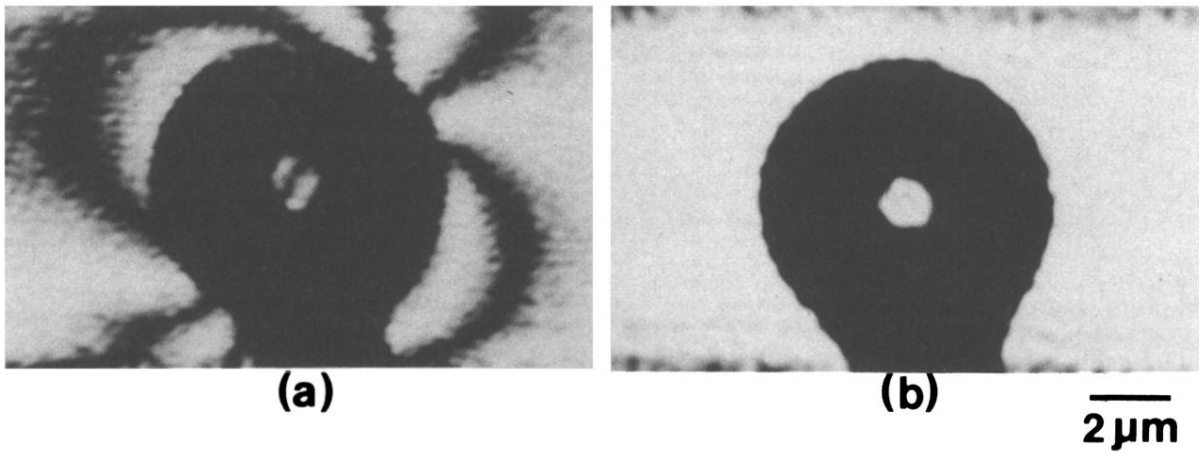


FIG. 8. Contour maps of toroidal magnets at room temperature. (a) Toroid with leakage field (phase amplification, $\times 2$). (b) Toroid without leakage field (phase amplification, $\times 2$).